# ALIGNMENT AND MERGING OF ELECTRON MICROSCOPE IMAGES OF FROZEN HYDRATED CRYSTALS OF THE T4 DNA HELIX DESTABILIZING PROTEIN GP32*I

ROBERT A. GRANT,* MICHAEL F. SCHMID,* WAH CHIU,* JAMES F. DEATHERAGE,* AND JUNKO HOSODA‡

*Department of Biochemistry and Department of Molecular and Cellular Biology, University of Arizona, Tucson, Arizona 85721; and ‡Lawrence Berkeley Laboratory, University of California, Berkeley, California 94721

ABSTRACT Low dose cryoelectron microscopy has been used to record images and electron diffraction patterns of frozen hydrated crystals of the single-stranded DNA binding protein gp32*I. Fourier transforms from 13 image areas, corresponding to ~40,000 unit cells, were aligned by a minimal phase residual search and merged by vector addition in reciprocal space. Phases from the resulting composite transform were combined with amplitudes from electron diffraction patterns to reconstruct the projected mass density of the gp32*I crystal at 8.4 Å resolution.

## INTRODUCTION

Gene 32 of the T4 bacteriophage codes for a protein, gp32 (33,500 mol wt), that binds tightly and cooperatively to single-stranded DNA (ssDNA). It has been shown that gp32 is required for replication, repair and recombination of the T4 genome in vivo (Alberts and Frey, 1970; Williams and Konigsberg, 1981). Removal of 50 amino acids from the carboxyl terminus of gp32 by limited proteolytic digestion produces the fragment gp32*I (27,000 mol wt) (Hosoda and Moise, 1978). Gp32*I retains the intact protein's ability to bind ssDNA cooperatively and can substitute for gp32 in an in vitro assay of leading strand synthesis (Burke et al., 1980). Under low salt conditions gp32*I crystallizes as thin platelets suitable for high-resolution electron diffraction analysis (Chiu and Hosoda, 1978). The space group of these crystals is $P2_12_12$ ($a$ = 47 Å, $b$ = 63 Å, $c$ = 90 Å). A low-resolution (20 Å) three-dimensional reconstruction of negatively stained gp32*I crystals has been reported (Cohen et al., 1983). Part of this low-resolution model has a shape similar to that of the ssDNA binding protein gp5 (9,700 mol wt) from the filamentous phage fd whose structure has been determined to 2.3 Å by x-ray crystallography (Brayer and McPherson, 1983).

Extension of the gp32*I structure determination to higher resolution by electron microscopy requires the use of low-temperature, low-dose imaging (Jeng and Chiu, 1984) and the protection of the crystals from drying in the vacuum of the microscope by embedding them in either glucose (Unwin and Henderson, 1975; Cohen et al., 1983) or ice (Taylor and Glaeser, 1974; Cohen et al., 1984). We have chosen ice embedding (the frozen hydration technique) because of the higher contrast at low resolution in images of frozen hydrated crystals compared to glucose-embedded crystals. This higher contrast at low resolution should facilitate the interpretation of the mass density map obtained by image analysis (Glaeser et al., 1979; Cohen et al., 1984).

Low dose electron microscope images of frozen hydrated gp32*I crystals are typically very noisy because of the poor statistics of image formation. The poor signal-to-noise ratio in this type of data can be overcome using Fourier averaging over many unit cells if crystals with sufficiently coherent long range order can be imaged (Kuo and Glaeser, 1975; Unwin and Henderson, 1975). If the crystal lattice is imperfect or distorted during specimen preparation, or if the image has significant pincushion or barrel distortion, Fourier averaging over large areas is unlikely to produce satisfactory results (Hayward and Stroud, 1981; Crepeau and Fram, 1981). An alternative to Fourier averaging over large areas is to align and merge smaller areas that are suitably coherent. Schemes for aligning and merging data from distorted lattices have been applied to high-dose images of imperfectly ordered, negatively stained arrays of biological interest (Saxton and Baumeister, 1982; Creapeau and Fram, 1981). In these procedures the distorted lattice is mapped out using correlation techniques and the average motif in the lattice is obtained by real-space averaging. This approach is facilitated by the high contrast in high dose images of negatively stained specimens. An alternative approach in which many Fourier averages from small areas were aligned and then merged in reciprocal space using a strategy based on the multiplica-

tion of phase probability distribution functions has been applied to low dose images of glucose-embedded purple membrane (Hayward and Stroud, 1981). We have developed a series of computer programs to align and merge Fourier averages of many small areas in which the data are merged by vector addition in reciprocal space. We report here our results at 8.4 Å nominal resolution from the application of these programs to images of frozen hydrated crystals of gp32*I.

## METHODS

### Specimen Preparation and Electron Microscopy

Procedures for the purification and crystallization of gp32*I have been published (Hosoda and Moise, 1978; Chiu and Hosoda, 1978). Frozen hydrated gp32*I crystals were prepared for electron microsopy by either sandwiching the crystal suspension between two thin carbon films (Jaffe and Glaeser, 1984) and freezing in liquid nitrogen (the "carbon sandwich" technique), or by rapid blotting of the suspension from a single carbon film (the "open-face" technique) and immediately freezing in liquid ethane (Lepault et al., 1983). In our hands the success rates for obtaining thin ice by these two methods have been about the same. The open-face method has the advantage that no evaporation of solvent is allowed to occur, so the concentration of solutes during specimen preparation is not a problem. The disadvantage of the open-face method is that a very concentrated crystal suspension must be used because most of the crystals are removed during the rapid blotting of the carbon substrate. Conversely, the carbon sandwich method can be used with more dilute crystal suspensions but the concentration of solutes during the air-drying step may be a problem, especially with a crystal like gp32*I that grows under low salt conditions. When we used the carbon sandwich procedure we would wash our crystals in distilled water before applying them to the grid. Our current preference is the open-face method because of the salt sensitivity of our crystals.

Frozen hydrated specimens were loaded into specimen holders under liquid nitrogen and transferred through a modified airlock (Taylor and Glaeser, 1973) to a JEM-100CX electron microscope (JEOL, Ltd., Tokyo, Japan). The microscope is equipped with a liquid nitrogen-cooled, high-resolution, top-entry configuration cold stage (Hayward and Glaeser, 1980). The stage is extremely stable, allowing us routinely to image the 3.44 Å spacing of graphitized carbon at low temperature. The cold stage was kept at ~130°K during imaging. In our early work with the cold stage we had problems with severe contamination of our specimens with condensed ice. We have improved the situation markedly by modifying the upper anti-contamination device of the microscope so that it is now colder (120°K) than the specimen. This has more than doubled the amount of time we can examine a specimen (~5 h for glucose-embedded specimens and ~1 h for frozen hydrated specimens) but ice condensation is still a factor that limits our efficiency in collecting high-resolution image data from frozen hydrated specimens.

Crystals embedded in suitably thin ice were located by scanning the grids in diffraction mode with the diffraction pattern defocused to produce a low-magnification, high-contrast image. The dose rate in diffraction mode was <1 e/Å$^2$-min. Once a suitable crystal was found, the diffraction pattern was focused and an electron diffraction pattern was recorded using ~1 e/Å$^2$. The microscope was then switched to magnification mode and focused on an area adjacent to the crystal. Care was taken to avoid irradiating the crystal of interest during focusing. A low dose image of the frozen hydrated crystal was then recorded at 40,000× magnification with a dose of 5–10 e/Å$^2$. This low-dose image was followed by two-high dose images (20–30 e/Å$^2$). The first high dose image was recorded at the same defocus as the low dose image, the second at a slightly greater defocus. These high dose images were used to determine the contrast transfer function of the microscope, which usually could not be determined from the low dose image (Jeng and Chiu, 1984).

### Image Processing

Images of frozen hydrated gp32*I crystals were evaluated by optical diffractometry. Images that produced optical diffraction patterns with diffraction maxima out to an isotropic resolution of at least 15 Å were digitized with a PDS 1010MS microdensitometer (Perkin-Elmer, Applied Optics Division, Garden Grove, CA) using either a 10 or 16 $\mu m^2$ aperture. Eighteen image areas of either 1024 × 1024 or 800 × 800 pixels were digitized from three different negatives. Fourier transforms of the 18 image areas were computed and displayed so that the transform could be indexed and the coordinates of the strongest reflections determined. The reciprocal lattice was refined for each transform; then amplitudes and phases were determined at reciprocal lattice positions out to 8 Å resolution. The phase of each reflection was corrected for contrast reversal due to the transfer function of the microscope, which was determined for each low-dose negative from the rings in the optical transform of the negative or its corresponding high-dose images (Thon, 1971). Reflections close to the nodes of the contrast transfer function, whose phases could not be corrected with confidence, were discarded.

The data were merged in three steps. First, the Fourier transforms from each of the three negatives were aligned and merged with other transforms from the same negative. Next, the shifts required to align the merged data from different negatives were determined. Finally, data from the different negatives were combined to produce the final composite map.

A composite transform for each negative was built up by stepwise addition of transformed image areas as outlined in Fig. 1. The transform with the best p2 symmetry was shifted to its best p2 origin and used as the starting template ($F_1$). A second transform ($F_2$) was aligned to the starting template by application of the appropriate phase shift. The two aligned transforms were then merged by vector addition of their complex structure factors. The resulting composite transform was used as the

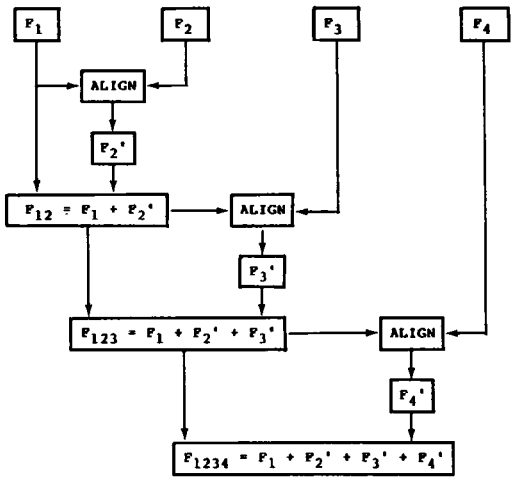


FIGURE 1 Flow diagram for the alignment and merging of images. The procedure is outlined for four images but can be used for more or fewer. $F_i$ represents the complex structure factors of image $i$ and $F_i'$ represents the same structure factors after they have been aligned to the template transform. The shift required to align two transforms is determined by searching for the shift that produced the minimum amplitude weighted root mean squared phase residual between the test transform and the template transform. This operation is represented by the ALIGN box. The test transform enters the ALIGN box from the right. The template transform enters the ALIGN box from the left. The addition of structure factors is vectorial.

template to align the next transform ($F_3$). The process was repeated until all transforms that could be aligned with confidence had been merged.

The shifts used to align the transforms at each step were determined by searching for the shift that produced the minimum amplitude-weighted root-mean-squared (RMS) phase deviation between the shifted and template transforms:

$$\mathrm{RMS}\,(x, y) = \sqrt{\Sigma F_2\,(\mathrm{h}, k)\,[\theta_1\,(h, k) - \theta_2\,(h, k)]^2 / \Sigma F_2\,(h, k)},$$

where $(h, k)$ is the Miller index of a reflection, $\theta_1$ and $\theta_2$ are the phases of the reflection from the template and shifted transforms, $F_2$ is the amplitude of the reflection from the shifted transform, and $x$ and $y$ correspond to the shift of the image along the unit cell axes in real space. The sum is over all reflections having acceptable phase coherence across the diffraction maximum and a peak-to-background ratio above three in the shifted transforms. This relatively high cutoff value was used only in the alignment step. All reflections were used in the vector addition step. For most alignments a unique minimum RMS residual was obtained, indicating that there was a single best alignment of the transforms. In cases where multiple minima were obtained, the transform being aligned was not merged with the template. Five transforms were eliminated from the data set for this reason. The same minimal RMS residual search was used to determine the best alignment of the composite transforms from the three negatives. After application of the appropriate phase shifts, data from different negatives were also merged by vector addition of complex structure factors from individual image areas. The resulting composite transform was then used as the template to refine the alignment of the individual transforms. This refinement step did not change the alignment of the individual images more than a few degrees on each axis of the unit cell. After three cycles of refinement the shifts for all the images converged to within one degree on each axis. A final composite transform was then calculated by vector addition of structure factors from 13 appropriately shifted transforms from the three negatives. These 13 transforms correspond to a combined total of ~40,000 unit cells.

Two electron diffraction patterns of frozen hydrated gp32*I crystals were digitized and the background intensity around each reflection was subtracted. Integrated intensities were calculated for reflections out to 5 Å resolution. The patterns were scaled to each other by Wilson scaling (Wilson, 1942), using 291 common reflections, and a single set of intensities was obtained by combining the two data sets.

The composite transform was shifted to its best p2 origin and p2 symmetry was enforced by setting each structure factors' phase to the nearest centrosymmetric value. A figure of merit equal to the cosine of the deviation of the raw phase from centrosymmetry was determined for each reflection. This figure of merit downweights the reflections acording to their deviation from centrosymmetry. Phases from 25 composite reflections that obeyed pgg symmetry were used to calculate the composite projection map. These phases were combined with amplitudes derived from the electon diffraction patterns to produce a set of structure factors corrected for the contrast transfer function of the microscope. These structure factors were used to calculate the pgg enforced composite projection map shown in Fig. 2. The 25 reflections used contain essentially all of the data out to 10 Å resolution plus a pair of reflections at 8.4 Å. In the projection map calculation each pgg related pair of refections was weighted by the average figure of merit of the pair. The average figure of merit of the map is 0.083.

## RESULTS

Well-focused low-dose images of frozen hydrated gp32*I crystals are featureless to the naked eye because of poor contrast transfer at low resolution but reveal the presence of periodicity when analyzed by optical diffractometry (Fig. 3). The highest resolution reflections visible in the optical diffraction patterns of the negatives processed were

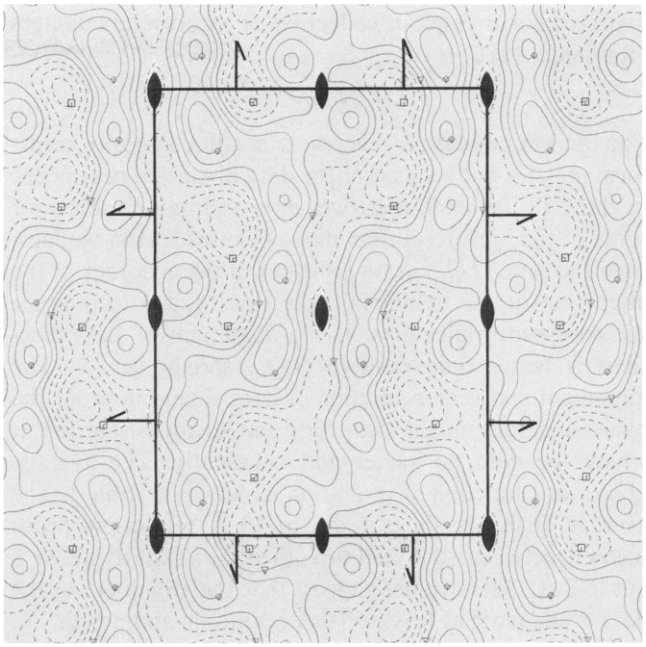

FIGURE 2 Pgg enforced projection map reconstructed from images of frozen hydrated gp32*I crystals. The phases for this reconstruction were obtained by the vector addition of 13 aligned Fourier transforms corresponding to ~40,000 unit cells. The average figure of merit is 0.083. The high density (protein) contours are solid and the low density (ice) contours are dashed. The protein dimer is well resolved. The projected unit cell (47 Å × 63 Å) is outlined. Twofold axes (●) and screw axes (↑) are indicated.

(3, 4), (4, 0) and (3, 3) at 11.1 Å, 11.8 Å, and 12.6 Å, respectively.

A comparison of the minimum RMS phase residual method of aligning data with the cross-correlation method showed that the two methods give essentially the same alignments. The RMS phase residual minima that gave the best alignments between image areas ranged from 30°–60°. The expected value of the RMS residual for a set of random deviations between 0° and 180° is 104°. The deviation of the RMS from this expected value can be used as a measure of the statistical significance of the alignment. The RMS calculation typically included ~20 common reflections. We estimate our typical RMS residual to be 3–5 standard deviations of the RMS residual from the expected value for two unrelated structures.

The phase coherence for any given reflection in the final composite transform can be measured using the factor:

$$Q\,(h, k) = \left|\sum_{i=1}^{m} F_i\,(h, k)\right| \Big/ \sum_{i=1}^{m} |F_i\,(h, k)|,$$

where $F_i(h, k)$ is the complex structure factor of reflection $(h, k)$ in the $i$th image and $m$ is the number of images being combined (van Heel and Hollenberg, 1980). The maximum possible $Q$ factor of 1 is obtained when the phases of all the structure factors being added are the same. In the absence of noise and systematic error, accurately aligned reflections should have a $Q$ factor of 1. The $Q$ factor

expected for a random collection of $m$ structure factors (Rayleigh, 1880) is

$$Q_{ran} = m^{-0.5}.$$

For the low-resolution reflections in the composite transform $m$ is 13, but because of the data discarded near nodes in the CTF for each negative, $m$ is as small as seven for some of the high-resolution data. For this reason we have used the ratio $Q{:}Q_{ran}$ as an indicator of the accuracy of the alignment of the individual reflections added to produce the composite reflections. If the alignment of the reflections is better than random $Q{:}Q_{ran}$ should be >1. The alignment and vector addition of data should improve the phase accuracy in the transform out to the resolution at which the data no longer add coherently. The average $Q{:}Q_{ran}$ as a function of resolution is shown in Table I. The average $Q{:}Q_{ran}$ is above 1 out to 10 Å resolution, drops below 1 between 10 Å and 9 Å, then rises slightly above 1 out to 8 Å. These values suggest that the alignment of the data is adequate at least to 10 Å resolution and possibly to 8 Å. The vector addition of structure factors for three representative composite reflections is shown in Fig. 4. Each panel contains an Argand diagram that shows the component vectors added to produce a single composite structure factor and the resulting vector average of the components.

The space group of the gp32*I crystal requires that images of untilted crystals have p2 symmetry. If adding images has actually improved the statistics of the data, then the p2 symmetry of the composite should be better than in the individual component images. The best p2 origin of the composite gave an amplitude-weighted p2 phase residual of 33°. The average amplitude-weighted phase residual of the individual images from the best p2 origin of the composite transform was 42°.

The pgg enforced composite projection map obtained by merging data from the 13 image areas is shown in Fig. 2. Two protein dimers per unit cell are well resolved as high-density regions in a low-density solvent (ice) matrix.

## DISCUSSION

The projection map obtained by the merging of data from different image areas (Fig. 2) has significantly better resolution than has been obtained from negatively stained crystals and is more consistent with the low-resolution three-dimensional structure than glucose maps at comparable resolution (Cohen et al., 1983). The low density contours (dashed lines in the map) correspond to the projection of stain filled solvent channels that have been observed in the low resolution three-dimensional reconstruction (Cohen et al., 1983). In a corresponding projection of negatively stained crystals the protein (stain-excluding area) is resolved as a single major peak per protein monomer (Cohen et al, 1984). In the composite structure of frozen hydrated crystals four major peaks per monomer have been resolved.

TABLE I
AVERAGE Q/Qran FOR THE COMPOSITE REFLECTIONS AS A FUNCTION OF RESOLUTION

| Resolution Range (Å) | Average Q/Qran |
|---|---|
| 70–25 | 2.07 |
| 25–15 | 1.94 |
| 15–12 | 2.01 |
| 12–10 | 1.42 |
| 10–9 | 0.81 |
| 9–8 | 1.13 |

The ratio is 1.00 for reflections that add with a phase consistency better than that expected for random phases. The low value for the 10 Å–9 Å range may be due to the low amplitudes of reflections in that zone. The data add with a phase coherence slightly better than random out to 8 Å resolution, indicating that the alignment is acceptable to about 8 Å.

We have developed our image alignment and adding procedure with the hope of improving the reliability of our phase determination from images and extracting as much resolution as possible from our data. Our procedure differs from that of Hayward and Stroud (1981) mainly in the way the data from different image areas are merged. Their approach is based on the assumption of a specific noise distribution in the data and relies on information about the expected amplitudes from diffraction patterns to prevent spurious noise peaks from dominating the merged data. Our merging of data by vector addition in reciprocal space is conceptually straightforward and assumes only that the data can be accurately aligned.

Rather than aligning all our data to a single template and then merging it in a single step, we used a stepwise approach because it allows each image area to influence the alignment of the areas added in after it. Stepwise

FIGURE 3 Optical diffraction pattern of an image of a frozen hydrated gp32*I crystal. The crystal was frozen in liquid ethane and imaged at 130°K. The highest resolution reflection (arrow) is (3, 4) at 11.1 Å.

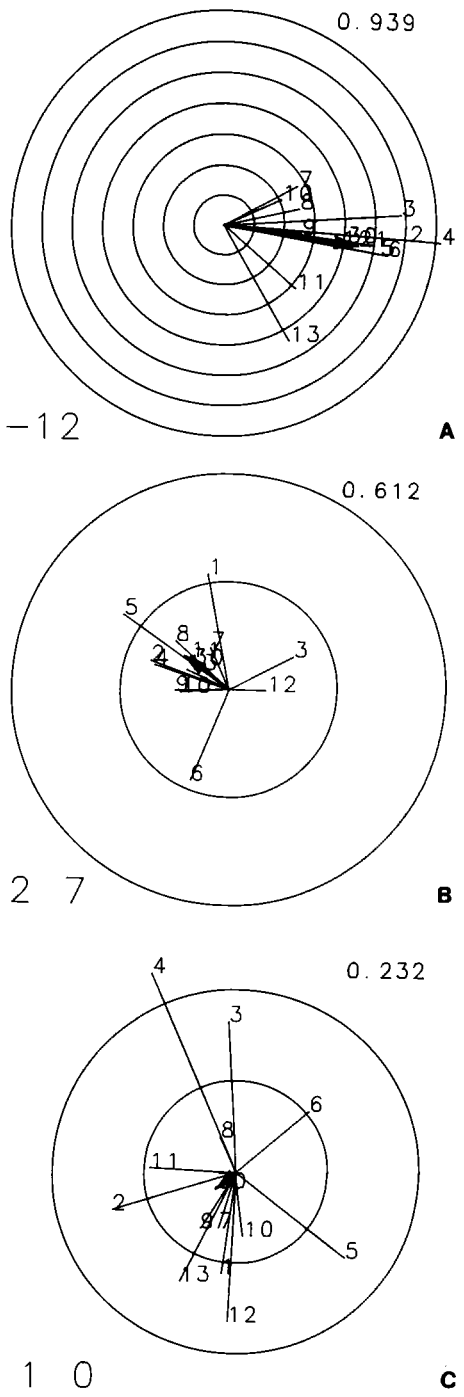


FIGURE 4 Each panel shows the Argand diagram that represents the vector addition if a given reflection from 13 images to produce a composite structure factor (bold arrow). The index of each reflection is shown in the *lower left* corner. The $Q$ factor in the *upper right* of each panel is a measure of the consistency of the phases of the structure factors being added. If all the phases are the same the $Q$ factor is one. The expected $Q$ factor for random phases ($Q_{ran}$) is 0.227 for each panel. The circles in each diagram represent equal increments in the amplitude of the reflections. Vectors pointing to the right have a phase of zero. (*A*) A strong, low resolution (26 Å) reflection adding coherently. (*B*) A weak reflection adding coherently. This reflection is the highest resolution reflection (8.4 Å) used to reconstruct the density map in Fig. 2 (*C*) A forbidden reflection adding incoherently. Please refer to the color figure section at the back of this book.

merging should also improve the signal-to-noise ratio of the template with each new image area added, thereby improving the accuracy of the alignment of the images added later. We have compared stepwise merging to one-step merging and found that it does result in slightly better phase coherence (as determined by the average $Q$ factor) in the composite image. It is possible that our results could be biased by the choice of the initial template. We have done the procedure several times, using different initial templates and the final maps have all been similar.

A critical step in any image-adding procedure is the alignment. High-resolution signal buried in noise should be retrievable from the addition of many noisy images if the alignment of the images is sufficiently accurate. The fact that the average $Q$:$Q_{ran}$ of the composite transform's structure factors is consistently above 1 out to 10 Å resolution suggests that the data add coherently and are therefore aligned at least to that resolution. The small rise in the ratio above 1 in the range 9 Å to 8 Å may not be significant, but our observation of a few high-resolution reflections that add coherently (e.g., Fig. 4 *b*) suggests that the alignment of the image areas is accurate enough for some new peaks to rise above noise level at high resolution. The improvement of the p2 symmetry of the composite image compared with the individual images shows that the accuracy of the phases is improved by merging the data, at least in the stronger reflections. This conclusion, however, is based on the assumption that the p2 origin of the composite image is the correct reference for all of the image areas. The relatively large p2 phase residuals we determined could be due to slight tilt of the crystals. Any difference in tilt could also affect the coherence of the vector addition of data from different crystals and therefore limit the resolution of the composite.

To extend our analysis to higher resolution we are in the process of incorporating two improvements into our data-processing procedures. These improvements are a cross-correlation step to map out the lattice distortion in an image so as to identify the most coherent regions for further processing, and the use of a real-space interpolation program (kindly provided by Dr. R. Henderson) that compensates for lattice distortions.

We are extending the analysis of frozen hydrated gp32*I crystals to three dimensions and expect to be able to determine the secondary structure of the molecule. A recent comparison of the sequences of six ssDNA binding proteins has revealed a structurally similar domain in each.[1] This domain is probably primarily $\beta$ structure. Specific residues are conserved at certain sites in all of the sequences. In the case of the gene 5 protein from bacteriophage fd, some of these sites have been suggested to be involved in direct contacts between the protein and the nucleic acid (Brayer and McPherson, 1984). A higher

[1]Prasad, B. V. V., and W. Chiu. Manuscript in preparation.

resolution three-dimensional structure of gp32*I may help confirm the predictions of this analysis.

We thank Dr. T. W. Jeng for valuable advice on low temperature imaging.

This work is supported by U. S. Public Health Services grant numbers GM27061 to W. Chiu and GM16841 to J. Hosoda, U. S. Department of Defense contract number DAMD17-84-C-4110 to W. Chiu, and U. S. Department of Energy contract number DEAC03-76SF00098 to J. Hosoda.

*Received for publication 6 May 1985 and in revised form 21 June 1985.*

## REFERENCES

Alberts, B. M., and L. Frey. 1970. T4 bacteriophage gene 32: a structural protein in replication and recombination of DNA. *Nature* (*Lond.* ). 227:1313–1318.

Amos, L. A. 1975. Combination of data from helical particles: correlation and selection. *J. Mol. Biol.* 99:51–73.

Brayer, G. D., and A. McPherson. 1983. Refined structure of the gene 5 DNA binding protein from bacteriophage fd. *J. Mol. Biol.* 169:565–596.

Brayer, G. D., and A. McPherson. 1984. Mechanism of DNA binding to gene 5 protein of bacteriophage fd. *Biochemistry.* 23:340–349.

Burke, R. L., B. M. Alberts, and J. Hosoda. 1980. Proteolytic removal of the COOH terminus of the T4 gene 32 helix-destabilizing protein alters the T4 in vitro replication complex. *J. Biol. Chem.* 225:11484–11493.

Chiu, W., and J. Hosoda. 1978. Crystalization and preliminary electron diffraction study to 3.7 Å of DNA helix-destabilizing protein gp32*I. *J. Mol. Biol.* 122:103–107.

Cohen, H. A., W. Chiu, and J. Hosoda. 1983. Structural analysis of T4 DNA helix destabilizing protein (gp3*I) crystal by electron microscopy. *J. Mol. Biol.* 169:235–248.

Cohen, H. A., T. W. Jeng, R. A. Grant, and W. Chiu. 1984. Specimen preparative methods for electron crystallography of soluble proteins. *Ultramicroscopy.* 13:19–26.

Crepeau, R. H., and E. K. Fram. 1981. Reconstruction of imperfectly ordered zinc-induced tubulin sheets using cross-correlation and real space averaging. *Ultramicroscpy.* 6:7–18.

Glaeser, R. M., W. Chiu, and D. Grano. 1979. Structure of the surface layer of the outer membrane of *Spirillum serpens*. *J. Ultrastruc. Res.* 66:235–242.

Hayward, S. B., and R. M. Glaeser. 1980. High resolution cold stage for the JEOL 100B and 100C electron microscopes. *Ultramicroscopy.* 5:3–8.

Hayward, S. B., and R. M. Stroud. 1981. Projected structure of purple membrane to 3.7 Å resolution by low temperature electron microscopy. *J. Mol. Biol.* 151:491–517.

Hosoda, J., and H. Moise. 1978. Purification and physicochemical properties of limited proteolysis products of T4 helix destabilizing protein (gene 32 protein). *J. Biol. Chem.* 253:7547–7555.

Jaffe, J. S., and R. M. Glaeser. 1984. Preparation of frozen hydrated specimens for high resolution electron microscopy. *Ultramicroscopy.* 13:373–378.

Jeng, T. W., and W. Chiu. 1984. Experimental strategy in three-dimensional structure determination of crotoxin complex crystal. *Ultramicroscopy.* 13:27–34.

Kuo, I. A. M., and R. M. Glaeser. 1975. Development of methodology for low exposure, high resolution electron microscopy of biological specimens. *Ultramicroscopy.* 1:53–66.

Lepault, J., F. P. Booy, and J. Dubochet. 1983. Electron microscopy of frozen biological suspensions. *J. Microscopy.* 129:89–102.

Rayleigh, L. 1880. On the resultant of a large number of vibrations of the same pitch and arbitrary phase. *Phil. Mag. Suppl.* 5. 10:73–78.

Saxton, W. O., and W. Baumeister. 1982. The correlation averaging of a regularly arranged bacterial cell envelope. *J. Microscopy.* 127:127–138.

Taylor, K. A., and R. M. Glaeser. 1973. Hydrophilic support films of controlled thickness and composition. *Rev. Sci. Instr.* 44:1546–1547.

Taylor, K. A., and R. M. Glaeser. 1974. Electron diffraction of frozen hydrated protein crystals. *Science* (*Wash. DC*). 186:1036.

Thon, F. 1971. Phase contrast electron microscopy. *In* Electron Microscopy in Material Science. U. Valdre, editor. Academic Press, Inc., New York. 571–625.

Unwin P. N. T., and R. Henderson. 1975. Molecular structure determination by electron microscopy of unstained crystalline specimens. *J. Mol. Biol.* 94:425–440.

van Heel, M., and J. Hollenberg. 1980. On stretching of distorted images of two-dimensional crystals. *In* Electron Microscopy at Molecular Dimensions. W. Baumeister and W. Vogell, editors. Springer-Verlag, Berlin. 256–260.

Williams, K. R., and W. H. Konigsberg. 1981. Structure-function relationships in T4 single-stranded DNA binding protein. *In* Bacteriophage T4. C. K. Matthews, E. M. Kutter, G. Mosig, and P. B. Berget, editors. American Society for Microbiology, Washington, DC. 82–89.

Wilson, A. J. C. 1942. Determination of absolute from relative x-ray intensity data. *Nature* (*Lond.*). 150:151.

# DISCUSSION

*Session Chairman*: Benno Schoenborn
*Scribes*: Thomas N. Earnest and John Smuda

SHARNOFF: How do you develop phases for the Fourier transforms of the digitized images?

GRANT: When you digitize an electron microscope image and compute its Fourier transform, you get both the amplitude and the phase (e.g., Unwin and Henderson, 1975).

MOORE: How do you decide how big the coherent patch is in one of your micrographs, and how do you deal with systematic differences between patches due to tilt, for example?

GRANT: Incoherent areas are identified by the program we use to refine our reciprocal lattice parameters and calculate the amplitude and phase at each reciprocal lattice position. The program takes a rough estimate of the parameters, then looks for peaks in the transform near the predicted

locations. When it finds a peak near a predicted reciprocal lattice position, it applies a number of tests to it to see whether it should be used to refine the reciprocal lattice. Split peaks or peaks with poor phase coherence across them are not used. If an area is not coherent, the program will find only a few good spots and we would reject that area. Areas ≥ 5,000 unit cells consistently failed to pass this test. We did not rigorously address the possibility of small amounts of tilt. As long as the angle between a* and b* was close to 90° and the ratio of their lengths was close to the expected value, we assumed the crystal was untilted. This test is not very sensitive to small changes in tilt, so tilt is definitely a factor that could be limiting our resolution.

LANGMORE: What are the sources of lattice distortion? Are they involved with the placement of these thin crystals on the carbon foil or the freezing process itself? Can you compare the distortion observed in a negative stain with crystalline ice embedding versus vitreous ice?

GRANT: The distortion could be caused by adsorption to the carbon substrate, by the freezing process, or by a phase transition in the ice after freezing. At the time these data were collected our cold stage was operating in the − 130 to − 140 °C range. At this temperature we cannot maintain the embedding ice in the vitreous state. Even if the specimen were frozen in liquid ethane, after being warmed in the cold stage it would have been transformed into crystalline ice. It is possible that the water in the crystals' solvent channels was vitreous, because the crystals did remain ordered to fairly high resolution (Milligan, Brisson, and Unwin, 1983. *Ultramicroscopy*. 13:1-3). Whether the interaction of the carbon or the effects of the ice contribute most to the distortion I cannot say. We have recently made further improvements to the anticontaminator of our JEOL microscope that allow us to view specimins at − 150°C. At this temperature we can ensure that the ice in the specimin is vitreous. It will be interesting to see if data from crystals in vitreous ice are better.

DORSET: I think perhaps that problems with small tilt could have been removed if you had put a more severe constraint using pgg symmetry rather than p2 symmetry for combining areas of your specimen, because the mm symmetry of the diffraction pattern (the optical transform) would ensure that you have the right orientation of the areas that you are combining. Because these are three-dimensional crystals, there is also a problem with the thickness of the samples and the consistency of diffraction data from these samples. I'm curious what thickness range you had and whether you've compared sets of electron diffraction intensities among several crystals.

GRANT: For the data I've presented here the crystals are nominally untilted, so we haven't really worried about the thickness problem. When we start processing three-dimensional data this will be a critical question. One of the approaches we've used to solve this problem is to take a low-magnification, high-contrast image of the crystal to get a thickness estimate.

DORSET: There is another technique that might be applicable, one that has been used in material science and seems to work well in proteins. Since you have a densely packed reciprocal lattice, you can slightly tilt the crystals so that you can measure the width of the Laue zones, and the width is determined by the $\text{sinc}^2$ broadening of the reciprocal lattice rods. This seems to work. Another comment I have is related to the reliability of the high-angle data. Based on our experience with lipids, we are always worried about the effects of slight bends in the crystal on the diffraction intensities. This will not affect the image but can have a significant effect on the electron diffraction data. It's hard to say *a priori* at what resolution this will effect things. Your projection distance is somewhere around 90 A. If you consider, for example, work by Henderson and Zemlin (*Ultramicroscopy*. In press.), resolving bacteriorhodopsin by doing cross-correlation averaging of their data in real space (based also on our experience with paraffin crystals), you can sweep a small sampling aperture across your Fourier-filtered image, and then see that there are slight changes in orientation. Otherwise, if you're sampling a big area by electron diffraction you are combining the whole image. If you have a large projection distance, these data may not represent the total contents of the unit cell and this is a real danger in interpretation (as was shown by John Cowley in 1961 for silicate structures: Cowley, 1961. *Acta Crystallog.* 14:920-927).

FRANK: Is the general procedure practical for doing this kind of work? Correlation averaging has been around for quite a while and your method seems to be a roundabout way to do correlation averaging with less convenience, since you have to find the area of coherence by doing a trial filtration only to find out it may not be the right area. So you insert a number of steps that may not be necessary. When you do correlation averaging, you start with a minimum area much smaller than the one you use, and that maps the entire image and tells you at every point where your lattice is. So correlation averaging seems to be a rational way of arriving at all unit cell locations.

I think that there might be one technique that eventually converges from all these different directions. I have no doubt that each of these approaches bring in some new and nice ideas. You used the Q factor as the criterion for where to stop the merging of reflections, and I thought that to apply a criterion of $Q/Q_{ran} > 1$ is too relaxed because at 1 you have complete random vector addition. What is the rationale of applying this threshold rather than a more cautious factor like 1.5 or 2? It's been our experience that using Q in the context of correlation averaging and single particle averaging that we need to apply a bigger safety factor to get reasonable results.

CHIU: Since submitting this paper we have incorporated a correlation procedure into our scheme to map out lattice distortions and select the most coherent regions for processing. Admittedly our selection of $Q/Q_{ran} > 1$ as a cutoff for the data sets our threshold at the noise level, but we used the phase constraints imposed by our crystals' pgg symmetry as an additional criterion for screening data to include in the reconstruction. The Fourier coefficients used to compute the reconstruction were weighted by a figure of merit equal to the cosine of the phase deviation from 0° or 180°. The average figure of merit of the map is 0.83.

STEWART: I think what you have done with frozen hydrated material is very impressive. It is quite obviously superior to negative staining, but there are other ways of preserving biological material to high resolution, one of which, as you note in your paper, is embedding in glucose. You have suggested that it is preferable to use frozen hydrated samples because you may get higher contrast at the resolution at which you are observing the objects. Have you compared the frozen hydrated samples to similar crystals embedded in glucose?

GRANT: We compared images of these crystals in three different embedding media: negative stain, glucose, and ice. With maps truncated at 20-A resolution for comparison, we see that negative stain and ice show the same features, although there is a contrast reversal, because ice is less dense than protein while negative stain is more dense. Glucose is

only slightly more dense than protein, so the higher-density regions of the protein are masked by the glucose, complicating the interpretation of maps reconstructed from images of the glucose-embedded crystals. (See Cohen et al., 1983 and 1984, in our references.)

STEWART: But when you go to high resolution, the density of the embedding medium is not an important constraint. At 20 Å things may be different, but what happens at 10 or 8 Å, as in this study?

CHIU: We have made a quantitative comparison of electron diffraction patterns of glucose- and ice-embedded crototoxin complex crystals (Cohen et al, 1984). We found that the amplitudes of the structure factors are quite different in the range 30–10 Å and similar between 10 and 4 Å.

STEWART: Many people would think that examining material in glucose is much easier than frozen hydrated samples. So one one would question why at high resolution you are using frozen hydrated samples.

CHIU: In this paper we do not deal with very high resolution, by our criteria. The current goal of this project is 8 Å. At this borderline resolution it is difficult to say which specimen preparation procedure is best. We have taken the conservative approach and decided to solve the structure in ice, in spite of the technical difficulties, to ensure that we get an interpretable result. But at 3.5 Å the easier method of glucose embedding is appropriate (Cohen, et al., 1984).

STEWART: With frozen hydrated samples, I have had great difficulty controlling the thickness of the ice layer. What effect does the thickness of the crystalline ice layer, which may be as high as 1,000 Å, have on scattering electrons in dynamic ways when the image is being formed at high resolution? Could this be a factor in the differences between glucose and ice?.

CHIU: The best way to think about this is to calculate the symmetry reliability factor ($R$) which relate the symmetry-related reflections in an electron diffraction pattern. Our best patterns have an $R$ factor of $\sim$ 7 or 8%. By that criterion the data are probably reliable.

SCHOENBORN: Do you have any special tricks for taking these crystals down to low temperature or do you just freeze them?

GRANT: The currently accepted best way to freeze specimens is in liquid ethane, a very efficient cryogen. You put the crystals on a grid and blot it with wet filter paper and that forms a very thin layer. The grid is immediately plunged into liquid ethane which is cooled by liquid nitrogen. You then transfer to a storage container under liquid nitrogen and then later to the microscope.

SCHOENBORN: So you introduce severe strain on the protein itself?

GRANT: It seems to work. You can record electron diffraction patterns that go out to 3.5 Å.